REPORT DOCUMENTATION PAGE

Form Approved OMB NO. 0704-0188

1. REPORT DATE (DD-MM-YYYY)	2. REPORT TYPE	3. DATES COVERED (From - To)
08-10-2016	Final Report	6-Jun-2013 - 5-Jun-2016

4. TITLE AND SUBTITLE
Supramolecular Disassembly for Sensing

5a. CONTRACT NUMBER
W911NF-13-1-0187

5b. GRANT NUMBER

5c. PROGRAM ELEMENT NUMBER
611102

6. AUTHORS
S. Thayumanavan

5d. PROJECT NUMBER

5e. TASK NUMBER

5f. WORK UNIT NUMBER

7. PERFORMING ORGANIZATION NAMES AND ADDRESSES
University of Massachusetts - Amherst
Research Administration Building
70 Butterfield Terrace
Amherst, MA 01003 -9242

8. PERFORMING ORGANIZATION REPORT NUMBER

9. SPONSORING/MONITORING AGENCY NAME(S) AND ADDRESS (ES)
U.S. Army Research Office
P.O. Box 12211
Research Triangle Park, NC 27709-2211

10. SPONSOR/MONITOR'S ACRONYM(S)
ARO

11. SPONSOR/MONITOR'S REPORT NUMBER(S)
63889-CH.11

12. DISTRIBUTION AVAILIBILITY STATEMENT
Approved for Public Release; Distribution Unlimited

13. SUPPLEMENTARY NOTES
The views, opinions and/or findings contained in this report are those of the author(s) and should not contrued as an official Department of the Army position, policy or decision, unless so designated by other documentation.

14. ABSTRACT
Supramolecular assemblies that predictably respond to environmental changes have been of great interest due to their applicability in many areas. The key motivation for this interest involves the enhanced selectivity by materials that respond to the concurrent presence of two or more stimuli. Most of the polymers and the resultant assemblies designed for this purpose are based on a single assembly. We were interested in designing a system, where we bring together two different supramolecular assemblies each of which are independently and synergistically responsive to two different stimuli

15. SUBJECT TERMS
supramolecular assemblies, sensing, disassembly, molecular recognition, responsive assemblies

16. SECURITY CLASSIFICATION OF:			17. LIMITATION OF ABSTRACT	15. NUMBER OF PAGES	19a. NAME OF RESPONSIBLE PERSON
a. REPORT	b. ABSTRACT	c. THIS PAGE			Sankaran Thayumanavan
UU	UU	UU	UU		19b. TELEPHONE NUMBER 413-545-1313

Report Title

Supramolecular Disassembly for Sensing

ABSTRACT

Supramolecular assemblies that predictably respond to environmental changes have been of great interest due to their applicability in many areas. The key motivation for this interest involves the enhanced selectivity by materials that respond to the concurrent presence of two or more stimuli. Most of the polymers and the resultant assemblies designed for this purpose are based on a single assembly. We were interested in designing a system, where we bring together two different supramolecular assemblies each of which are independently and synergistically responsive to two different stimuli.

Enter List of papers submitted or published that acknowledge ARO support from the start of the project to the date of this printing. List the papers, including journal references, in the following categories:

(a) Papers published in peer-reviewed journals (N/A for none)

Received		Paper
07/14/2015	6.00	Conghui Yuan, Ying Chang, Jie Mao, Shirong Yu, Weiang Luo, Yiting Xu, S. Thayumanavan, Lizong Dai. Supramolecular assembly of crosslinkable monomers for degradable and fluorescent polymer nanoparticles, J. Mater. Chem. B, (02 2015): 2858. doi: 10.1039/C4TB01880J
07/14/2015	5.00	Cunfeng Song, Longyu Li, Matthew Jennings, S. Thayumanavan. Photoinduced heterodisulfide metathesis for reagent-free synthesis of polymer nanoparticles, Chem. Commun., (11 2014): 1425. doi: 10.1039/C4CC08000A
07/14/2015	7.00	Krishna R. Raghupathi, Jing Guo, Oyuntuya Munkhbat, Poornima Rangadurai, S. Thayumanavan. Supramolecular Disassembly of Facially Amphiphilic Dendrimer Assemblies in Response to Physical, Chemical, and Biological Stimuli, Accounts of Chemical Research, (06 2014): 2200. doi: 10.1021/ar500143u
09/09/2014	1.00	Conghui Yuan, Kishore Raghupathi, Bhooshan C. Popere, Judy Ventura, Lizong Dai, S. Thayumanavan. Composite supramolecular nanoassemblies with independent stimulus sensitivities, Chemical Science, (09 2013): 229. doi: 10.1039/c3sc52347k
TOTAL:	**4**	

Number of Papers published in peer-reviewed journals:

(b) Papers published in non-peer-reviewed journals (N/A for none)

Received		Paper
09/09/2014	4.00	Longyu Li, Kishore Reddy Raghupathi, Cunfeng Song, Priyaa Prasad, S. Thayumanavan. Self-assembly of Random Copolymers, Chem. Commun., (06 2014): 0. doi:

TOTAL: **1**

Number of Papers published in non peer-reviewed journals:

(c) Presentations

Number of Presentations: 0.00

Non Peer-Reviewed Conference Proceeding publications (other than abstracts):

Received	Paper

TOTAL:

Number of Non Peer-Reviewed Conference Proceeding publications (other than abstracts):

Peer-Reviewed Conference Proceeding publications (other than abstracts):

Received	Paper

TOTAL:

Number of Peer-Reviewed Conference Proceeding publications (other than abstracts):

(d) Manuscripts

Received		Paper
09/09/2014	2.00	Sompit Wanwong, Ambata Poe, Ganapathy Balaji, S. Thayumanavan. The effect of heteroatom conformation on optoelectronic properties of cyclopentadithiophene derivatives, Organic & Biomolecular Chemistry (02 2014)
09/09/2014	3.00	Krishna R. Raghupathi, Jing Guo, Oyuntuya Munkhbat, Poornima Rangadurai, S. Thayumanavan. Supramolecular Disassembly of Facially Amphiphilic Dendrimer Assemblies in Response to Physical, Chemical, and Biological Stimuli, Accounts of Chemical Research (07 2014)
TOTAL:		**2**

Number of Manuscripts:

Books

Received	Book
TOTAL:	

Received	Book Chapter
TOTAL:	

Patents Submitted

Patents Awarded

Awards

CRSI Medal, Chemical Research Society of India (2016)
Chancellor's Medal, University of Massachusetts (2014)

Graduate Students

NAME	PERCENT_SUPPORTED	Discipline
Celia Homyak	0.37	
Bin Liu	0.65	
Priyaa Prasad	0.12	
Poornima Rangadurai	0.37	
Bo Zhao	0.18	
Jiaming Zhuang	0.29	
Mallory Gordon	0.05	
FTE Equivalent:	**2.03**	
Total Number:	**7**	

Names of Post Doctorates

NAME	PERCENT_SUPPORTED
FTE Equivalent:	
Total Number:	

Names of Faculty Supported

NAME	PERCENT_SUPPORTED	National Academy Member
Sankaran Thayumanavan	0.07	
FTE Equivalent:	**0.07**	
Total Number:	**1**	

Names of Under Graduate students supported

NAME	PERCENT_SUPPORTED
FTE Equivalent:	
Total Number:	

Student Metrics

This section only applies to graduating undergraduates supported by this agreement in this reporting period

The number of undergraduates funded by this agreement who graduated during this period: 0.00

The number of undergraduates funded by this agreement who graduated during this period with a degree in science, mathematics, engineering, or technology fields:..... 0.00

The number of undergraduates funded by your agreement who graduated during this period and will continue to pursue a graduate or Ph.D. degree in science, mathematics, engineering, or technology fields:..... 0.00

Number of graduating undergraduates who achieved a 3.5 GPA to 4.0 (4.0 max scale):..... 0.00

Number of graduating undergraduates funded by a DoD funded Center of Excellence grant for Education, Research and Engineering:..... 0.00

The number of undergraduates funded by your agreement who graduated during this period and intend to work for the Department of Defense 0.00

The number of undergraduates funded by your agreement who graduated during this period and will receive scholarships or fellowships for further studies in science, mathematics, engineering or technology fields:..... 0.00

Names of Personnel receiving masters degrees

NAME
Total Number:

Names of personnel receiving PHDs

NAME
Jiaming Zhuang
Total Number: 1

Names of other research staff

NAME	PERCENT_SUPPORTED
FTE Equivalent:	
Total Number:	

Sub Contractors (DD882)

Inventions (DD882)

Scientific Progress

Please see attachment

Technology Transfer

Final Report for the U.S. Army Research Office

Supramolecular Disassembly for Sensing

Submitted by: S. Thayumanavan to Dr. Dawanne Poree and Wendy Mills (ARO)
October 2016

First Year Progress:

Supramolecular assemblies that predictably respond to environmental changes have been of great interest due to their applicability in many areas. The key motivation for this interest involves the enhanced selectivity by materials that respond to the concurrent presence of two or more stimuli. Most of the polymers and the resultant assemblies designed for this purpose are based on a single assembly. We were interested in designing a system, where we bring together two different supramolecular assemblies each of which are independently and synergistically responsive to two different stimuli. To this end, we have developed a new reactive self-assembly route in which we achieve a dynamic composite nanostructure, where a redox sensitive nanogel is coated over a pH sensitive block polymeric micelle (Fig. 1). To fully test versatility of the approach, we stipulated that: (*i*) both micelle and nanogel should preserve their morphological fidelity in the composite assembly; (*ii*) the constituent nanoassemblies independently respond to their respective stimuli; and (*iii*) at least one synergistic feature of the composite nanoassembly is demonstrated.

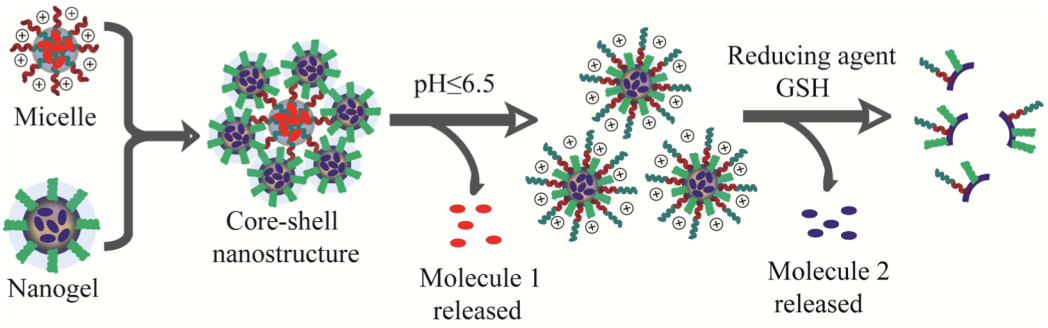

Fig.1. Schematic representation of the composite nanostructure assembly and stimuli-sensitive disassembly.

The composite nanostructure is based on a micellar assembly formed from an amphiphilic block copolymer and a nanogel formed from a self-crosslinking polymer assembly. Specifically, poly(2-(diisopropylamino)ethylmethacrylate-*b*-2-aminoethyl methacrylate hydrochloride) ($PDPA_{30}$-b-$PAMA_{15}$) is used as the block copolymer, which was synthesized by atom transfer radical polymerization (ATRP) (Scheme 1). Similarly, nanogels were prepared from the random copolymer, poly(oligoethyleneglycolmonomethylether methacrylate-co-glycidylmethacrylate-co-pyridyldisulfideethylmethacrylate) (P(EGMA- GMA-PDSEMA)). The PDSEMA monomer was then used to generate disulfide crosslinks using D,L-dithiothreitol (DTT) using the procedures previously reported. Here, the EGMA monomer provides a charge-neutral hydrophilic group for self-assembly in aqueous phase, while the epoxide functionality in the GMA co-monomer provides the functional handle for reactive self-assembly with the block copolymer assembly (Scheme 1).

Prior to generating the composite nanoassemblies, we characterized the individual supramolecular assemblies generated from the block copolymer and the nanogel using dynamic light scattering (DLS). DLS studies of the block copolymer assembly revealed that the assemblies' diameters range from 10 to 35 nm (Fig.2B). Since certain amount of dilution would occur during the formation of these composite assemblies, the block copolymer assemblies were examined before and after dilution. The assemblies had small perturbations, if any, in size after diluting the solution to half concentration. Similarly, DLS characterization of the nanogels revealed sizes of ~10 nm in size (Fig. 2C). Transmission electron microscopy (TEM) was also used to further characterize the block copolymer micelles and the nanogels (Fig. 2D-2G).

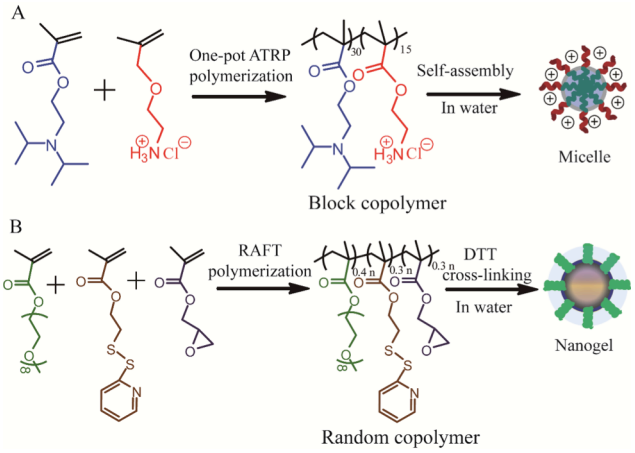

Scheme 1. Syntheses of the (a) PDPA30-b-PAMA15 block copolymer and (b) P(EGMA-GMA-PDSEMA) random copolymer and the corresponding nanogel.

Next, the possibility of obtaining composite nanostructure using the combination of polymer micelles and the nanogels was investigated. Under the reaction conditions, the amine moiety can open the epoxide ring to form the corresponding amino alcohol product. This reaction should covalently attach the micellar assembly and the nanogel. The fidelity of the resultant composite nanostructure was first tested by using micelles and nanogels both with ~10 nm in size. The reason for this choice is that these two assemblies with such diameters exhibit a narrow polydispersity in particle size. Although the micelle and the nanogel independently are ~10 nm in size, the composite nanostructure was found to be ~35 nm (Fig. 3A). The structure of the composite nanostructure was hypothesized to be a simple coating of nanogels on the micelle via covalent bonds.

To test this hypothesis, the composite nanostructures were investigated by TEM. In order to distinguish the micelle from the nanogel, we used: (*i*) a 25 nm micelle was used along with the 10 nm nanogel; and (*ii*) the heavy atom bearing dye molecule, BDP-C12-I2, for it to be non-covalently incorporated into the polymer micelle or the nanogel. The purpose of the latter dye as the guest molecule is to conveniently visualize the assembly in which the guest molecule is present. We envisioned that this guest molecule would act as a stain in TEM due to the heavy iodine atoms present in the molecule. If our hypothesis that the combination of the nanogel and the block copolymer assembly forms a

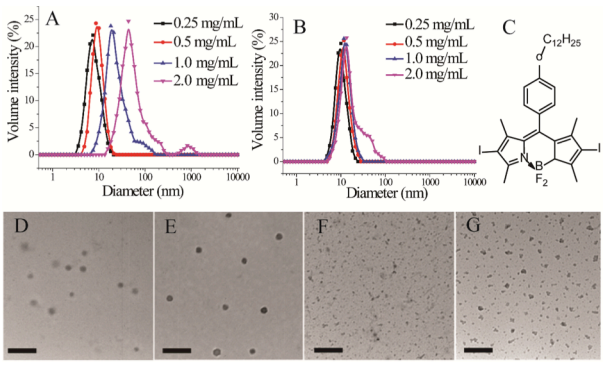

Fig. 2. (A) Dynamic light scattering (DLS) of micelles assembled from diblock copolymers at various concentrations; (B) DLS of nanogels at different concentrations; (C) chemical structure of BDP-C12-I2. TEM images of micelles before (D) and after (E) encapsulation of BDP-C12-I2, and nanogels before (F) and after (G) encapsulation of BDP-C12-I2.

composite type nanostructure, then when the dye molecule was incorporated into the nanogel, the shell should be darker and a hollow core should be observed (Fig. 3B). On the other hand, when the guest molecule is present in the micelle, a dark core coated with a lighter shell should be present. Indeed, TEM images are consistent with these expectations (Fig. 3B and 3C), thereby supporting our structural hypothesis. The difference in contrasts in these two structures also show that there is very little guest molecule transfer, if any, from one assembly to the other in the composite nanostructure.

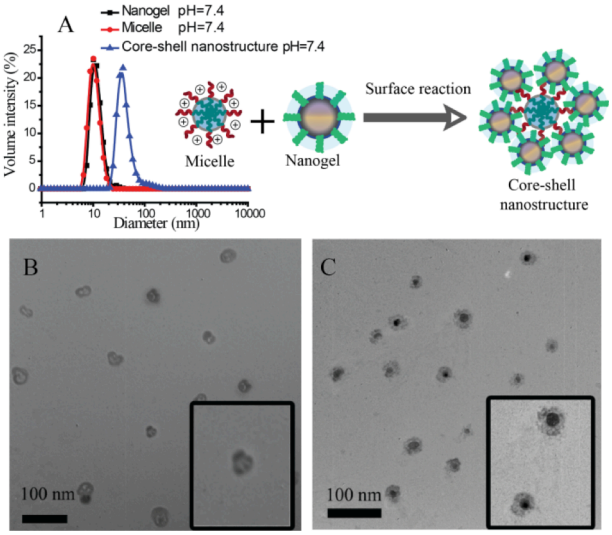

Fig. 3. (A) Dynamic light scattering of nanogels (■), micelles (●) and composite nanostructures at pH=7.4 (▲); the nanogels and the micelles were made from 0.5 mg/mL of random copolymer and block copolymer PDPA30-b-PAMA15 respectively; Inset in (A) schematically illustrates the morphology of the composite nanostructure. (B) and (C) are TEM images of compositenanostructures formed from the combination of nanogels and micelles; for the sample preparation of (B), the nanogels were loaded with BDP-C12-I2 while the micelles were empty to enhance their contrast; for the sample preparation of (C), the micelles were loaded with BDP-C12-I2 while the nanogels were empty to enhance their contrast.

Next, we tested the fidelity of the individual nanoassemblies, in terms of their stimuli-sensitive characteristics. Indeed, we noted that the BCP micelle retained its pH-sensitive behavior, while the nanogel retained its redox-sensitive behavior. We were able to show that these assemblies retained their behavior through pH-responsive fluorescence changes and redox-responsive fluorescence changes due to the molecules encapsulated within their respective assemblies.

Finally, we demonstrate the possibility of synergy in combining two nanostructures using an example. It is well known with many nanoscale architectures with positively charged surfaces are capable of being taken up by cells faster than anionic or charge-neutral assemblies. Note that the surface charge of the composite nanostructure is very similar to that of the nanogel itself. Therefore at pH 7.4, the composite nanoassembly should not have significant cellular uptake. However, when the pH is reduced at 6.5, the micelle at the core disassembles leaving behind the positively charged protonated tertiary amine block on the surface of the nanogel, which renders the nanogel positively charged (see Fig. 1 for an illustration). Therefore, at this pH the nanocomposite should exhibit a significant cellular uptake. We performed cellular uptake experiments with HeLa cells for 30

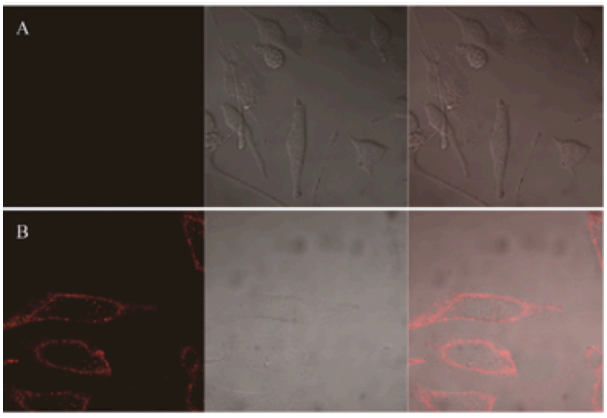

Fig. 4. Cell uptake of composite nanoassemblies at (A) pH 7.4 and(B) pH 6.5 after incubation with cells for 30 min. The composite nanoassemblies used in the dye release testing and cell uptake experiment were made from 9:1 ratio of copolymer 1 nanogels (40% crosslinked, 0.5 mg/mL) and $PDPA_{30}$-b-$PAMA_{15}$ micelles (0.5 mg/mL).Among each set of confocal images: left panel correspond to DiI emission, middle panel correspond to DIC image and right panel shows an overlap of both

minutes (Fig. 4A and 4B). No cellular uptake was observed at pH 7.4, whereas significant uptake was observed at pH 6.5. To insure that the nanogels themselves do not have any pH-dependent uptake, we carried out the control experiments with the nanogels themselves at both pHs. There was no discernible cellular uptake of the nanogels under both of these conditions. Strategies for pH-induced surface charge changes have been previously reported. The strategy outlined here, based on composite nanoassemblies, is based on fundamentally different approach.

In summary, we have shown that two different supramolecular nanostructures can be brought together to form a composite nanoassembly using a reactive self-assembly approach. We have shown that: (*i*) the composite nanostructures can be formed with the block copolymer assembly as the core and the nanogel as the shell; (*ii*) the relative placement of these assemblies can be ascertained by encapsulating a heavy-atom based guest molecule selectively in either nanostructure as a TEM stain; (*iii*) the stimuli-sensitive host-guest properties of the two assemblies are retained in the composite nanoassembly; (*iv*) the presence of nanogel as the shell around the block copolymer assembly causes a change in the overall surface charge; (*v*) the surface charge change results in reduced cytotoxicity of the composite nanostructure, relative to the block copolymer assembly; and (*vi*) the pH-sensitive disassembly of the block copolymer changes the surface of the nanogel to be cationic, which results in an enhanced cellular uptake of the nanoassembly at lower pH. The possibility of charge generation and guest molecular release in response to two different triggers, in the current system, highlights the possible utility of this type of composite nanoassemblies in many areas including diagnostics and sensing.

Second Year Progress:

A variety of intermolecular interactions have been extensively employed in the self-assembly of building blocks in various scales and have been explored for a variety of applications. Hydrogen bonding, hydrophobic aggregation, π-π stacking, coordination, electrostatic interaction are just a few popular examples of these interactions. Among these, coordination-based interactions have attracted i nterest due to their versatility in control over the directionality and strength of interactions. However, self-assembly due to strong coordination is not the preferred strategy for developing smart materials, as they can be often irreversible features. We were interested in developing a system, where small molecules are designed to self-assemble into nano-sized architectures due to weak, but reversible intermolecular B-N coordination.

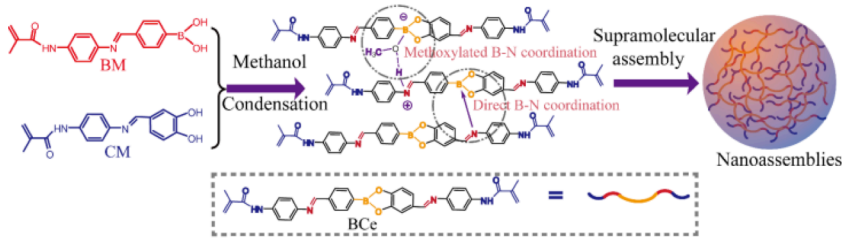

Scheme 1 Synthesis and supramolecular assembly of BCe.

Boronic acids with covalently appended neighboring nitrogenous groups form intramolecular B-N interaction worth ~13.0 kJ/mol. Intermolecular B-N dative bonds t can bring molecules together to form dimers or linear polymers or crosslinked structures. However, well-defined nanostructures through self-assembly driven by intermolecular B-N coordination requires the cooperation of secondary reinforcement such as π–π stacking and hydrogen bonding. Our previous collaborative work with L. Dai (Xiamen University) has shown that uniform

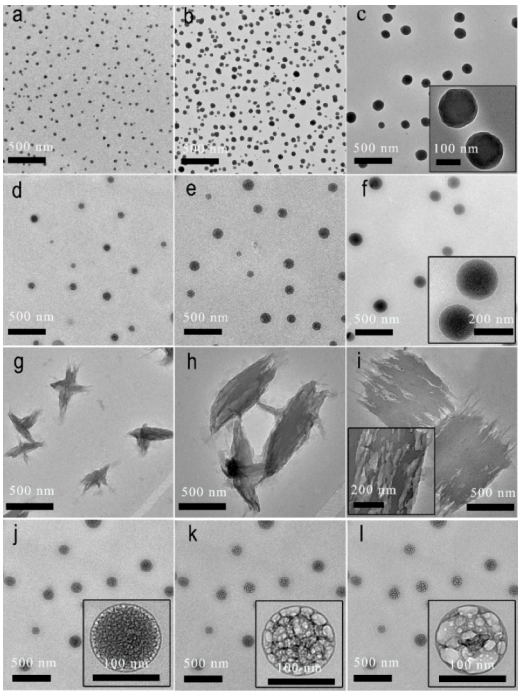

Fig. 1 TEM images of spherical nanoparticles prepared at -10 °C with (a) 10.0, (b) 20.0 and (c) 40.0 mM of BM and CM. (d), (e) And (f) represent the typical TEM images of spherical supramolecular assemblies obtained at 0 °C from 10.0, 20.0 and 40.0 mM of BM and CM, respectively. (g), (h) And (i) are the TEM images of layered structures formed by cooling the BCe methanol solution with 10.0 20.0 and 40.0 mM concentrations from 25 to -10 °C. (j), (k) And (l) show the morphologies of the spherical assemblies after electron beam irradiation for 30.0, 60.0 and 120 s, respectively; these nanospheres were prepared by using 20.0 mM of BM and CM at 0 °C. The insets are the corresponding magnified TEM images.

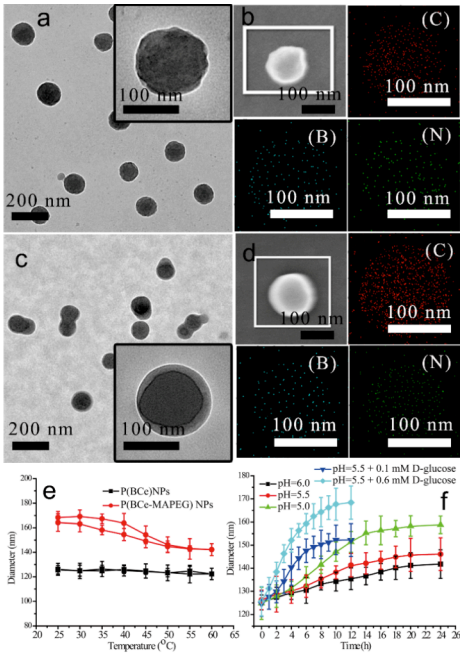

Fig. 2 (a) TEM images of P(BCe) NPs prepared from the photo polymerization of spherical assemblies at -10 °C, these assemblies were formed by using (a) 40.0 mM of BM and CM. (b) Typical SEM of a P(BCe) NP and EDX elemental mapping (C, B and N) of the nanoparticle. (C) TEM image of P(BCe-MAPEG) NPs prepared by using BCe assemblies that were obatined from (d) 40.0 mM of BM and CM. (d) Typical SEM of a P(BCe-MAPEG) N and EDX elemental mapping (C, B and N) of the nanoparticle. (e) Diameter evolution of P(BCe) NPs in water solution at neutral pH under thermal cycling. (f) Diameter evolution of P(BCe) NPs in acidic water solution or in the presence of D-glucose with pH=5.5

particles can only be formed through a combination of condensation polymerization and B-N coordination (Macromolecules, **2014**, *47*, 5869-5876).

We envisioned that the formation of multiple intermolecular B-N coordination would reinforce intermolecular interactions. To test this p ossibility, we targeted a boronic acid molecule (BM) and a catechol molecule (CM) shown in Scheme 1. A simple condensation reaction between these affords a planar boronate ester (BCe). The aim of this design is to not only explore the possible formation of multiple B-N coordination among BCe molecules, but also to endow the resultant supramolecular assemblies with responsive characteristics to pH and carbohydrates. The introduction of polymerizable bonds into the boronate ester makes it possible to crosslink and functionalize these assemblies, which circumvents any pre-mature disassembly of the BCe assemblies in the aqueous phase. We show that the degradation of BCe monomer and the polymerized nanoassemblies under the stimuli of acidic pH or D-glucose, is accompanied with a dramatic evolution of fluorescence character.

We were interested in testing whether BCe assemblies resulted in the formation of controlled nanoparticles. Indeed, when the condensation was carried out at -10 °C in methanol, nanospheres with uniform size distribution were o btained, as characterized by the transmission electron microscopy (TEM) (Fig. 1a-c and the inset of Fig. 1c). We noted that there is a strong

correlation between the particle size of the assemblies and the concentration of the reactants. BCe assemblies prepared from 10.0, 20.0 and 40.0 mM of BM and CM show diameters from 38±4, 62±12 to 118±15 nm (statistical analysis of 100 particles), which have also been confirmed by the results of dynamic light scattering. A control experiment performed with boronate esters that are not capable of intermolecular B-N coordination did not produce any nanospheres.

Interestingly the BCe nanosphares formed at 0 °C were found to be more transparent than those from -10 °C (Fig. 1d-f and the inset of Fig. 1f). The concentration of BM and CM is also crucial in tuning the size of these assemblies, as evidenced by the successful preparation of BCe nanospheres with diameters ranging from 72±10, 122±22 to 180±28 nm (Fig. 1d-f). We then tried a special method for the self-assembly of BCe, in which BCe was synthesized at room temperature before cooling its methanol solution to -10 oC. Surprisingly, such a self-assembly route leads to an unexpected layered structure (Fig. 1g-i and the inset of Fig. 1i). However these nanostructures were quite fragile as shown in Figs. 1j-1l. Therefore, we resorted to stabilize the as-formed nanoparticles using photo-crosslinking reaction, where the polymerizable double bonds in the substrate molecules serve as the handle. The stabilization of these particles is illustrated by the TEM and SEM of the crosslinked particles shown in Fig. 2.

Since BM, CM and BCe are based on conjugated building blocks, we were interested in evaluating their photophysical properties as well. While not fluorescent at higher pH, BCe shows a strong green emission with a maximum of 480 nm in water (pH≤6.5) under the excitation at wavelength of 360 nm. The quantum yield (ϕ) of BCe in water with pH=5.5 was measured to be 0.50 by using 4', 6-diamidino-2-phenylindole (ϕ=0.58) as standard. The control building block molecules however did not exhibit any appreciable fluorescence. The fluorescence of BCe in water is highly pH-dependent, where a significant increase in emission intensity with decreasing pH (Fig. 3a and b). This enhancement is saturated at ~pH 5.5 (Fig. 3c). The fluorescence change seems to be recyclable (Fig. 3d), suggesting that the protonation-based event as the reason for the change in fluorescence. Neutralizing the BCe solution from pH=5.5 to 7.4 reduces or even quenches the fluorescence emission, whereas acidifying the neutral solution back to pH=5.5 can recover the fluorescence emission. After several cycles, the maximum emission intensity of BCe at pH=5.5

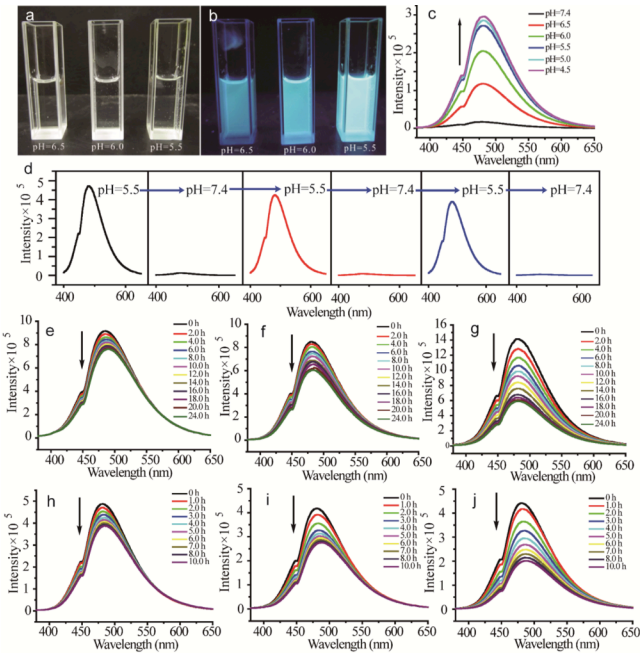

Fig. 4 Photographs of BCe in water with different pH under (a) natural light and (b) UV irradiation (wavelength 360 nm). (c) Effect of pH on the fluorescent emission intensity of BCe in water under an excitation wavelength 360 nm. (d) Switchable fluorescent emission of BCe in water when cycling the pH between 5.5 and 7.4. (e), (f) And (g) represent the emission evolution of BCe in water with pH=6.0, 5.5 and 5.0. (h), (i) And (j) trace the emission decays of BCe in water at pH=6.0 with 0.1, 0.2 and 0.6 mM of D-glucose, respectively.

exhibits a certain decline. We attribute this to the pH induced degradation of BCe, because both boronate and the imine moieties are dynamic and degradable in acid solution (Fig. 3e-g). In comparison to the control, BCe shows a much faster decay of emission intensity upon the addition of D-glucose (Fig. 3h-j). The emission intensities of BCe solutions at pH 6.0 in the presence of 0.1, 0.2 and 0.6 mM of D-glucose show reductions of 22, 34 and 54 % (calculated from Fig. 3h-j) respectively, but these responses have been slow.

Simiarly, we have also developed a reagentless synthesis of a responsive polymer nanoparticle, the results of which have been published. In summary, we have shown that intermolecular B-N dative bonding can provide a facile route to the supramolecular assemblies with controllable sizes. These assemblies can be stabilized and functionalized through a simple in-stiu photo polymerization. The versatility of the polymerized assemblies have been demonstrated by using this as a fluorescence reporter for pH or D-glucose activity changes. These highlight the possible utility of this type of composite nanoassemblies in many areas including diagnostics and sensing.

Final Year Progress:

Hybrid organic-inorganic nanomaterials for sensing applications: Nanomaterials for sensing are tremendously enhanced by high surface area nanomaterials. While nanoparticles already have this as an inherent advantage, a significant further step would involve the generation of hollow nanoparticles, where the surface area is even more enhanced. If organic-inorganic hybrid nanomaterials could be generated with these characteristics, then the impact could be even higher, because the sensing strategies that are possible through functionalization of organic materials can be combined with the catalysis opportunities that inorganic compounds provide. Majority of current nanomaterials are either purely inorganic, such as silica nanoparticles, metal and metal oxide nanocrystals, or purely organic, such as polymer nanoparticles and supramolecular assemblies. There is a recent surge in methods for generating hybrid metal-organic coordination materials, constructed from metal ions and polyfunctional organic ligands. One of the important determinants of their versatility emanates from the opportunity for diversity in these materials through functional group variations of the inorganic or organic building blocks.

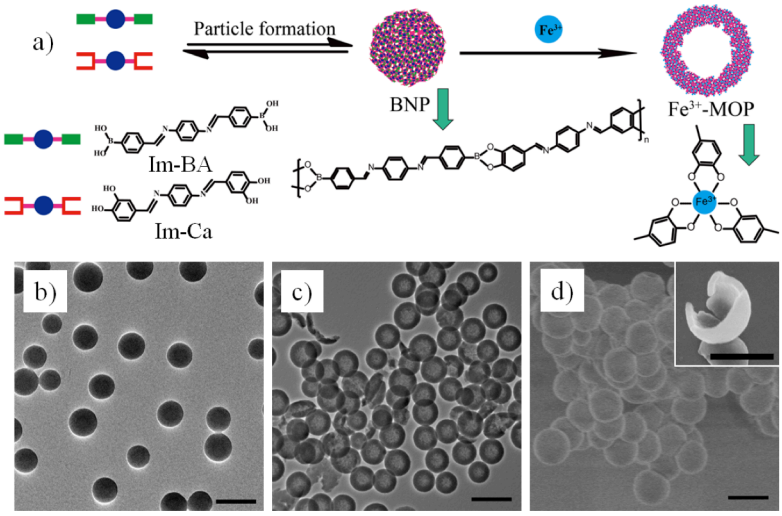

Figure 1. Boronate nanoparticles (BNP) and hollow metal organic nanoparticles (MOP) characterization. a) Scheme presents the syntheses of BNP via Im-Ca and Im-BA, and the preparation of hollow MOP by adding metal chloride salts to the BNP solution. b) TEM image of the BNP; c) TEM image of the hollow Fe^{3+}-MOP; d) SEM image of the hollow Fe^{3+}-MOP; Inset is a SEM image of one broken hollow Fe^{3+}-MOP. All the scale bar is 500 nm.

This chemical design feature has opened up the opportunities for these materials in a number of diverse applications such as catalysis, gas storage, biosensing, and biomedicine. In all these

applications, hollow nanoparticles have increasingly attracted special interest, because of their low density, high surface area, material economy, and lower cost compared to their solid counterparts. In this work, we report a simple, rapid, and robust strategy for achieving hollow MOPs, where we exploit the reversibility of the polymer backbone linkages through a simple addition of metal ions into the solution of well-defined polymeric nanoparticles. We show that: (*i*) the size of the hollow MOPs can be easily tuned by using the precursor organic polymer nanoparticles of different sizes; (*ii*) control over the thickness of the nanoparticle walls are achieved by the concentration of metal ions; (*iii*) the underlying mechanism for the formation of the hollow MOP is controlled by the relative diffusion of the reactive species in solution *vs.* the substrate polymer nanoparticle; and (*vi*) a variety of metal ions with different coordination geometries can result in the formation of the hollow MOPs, indicating the generality of the methodology.

Precursor organic boronate nanoparticles (BNP) can be achieved using a simple condensation-driven cooperative polymerization of a bis-imido boronic acid (Im-BA) molecule and a bis-imido catechol (Im-Ca) molecule in methanol, previously reported in 2014 by us. We explored the possibility of utilizing the strong interaction between Fe(III) species and catechols to interrupt the polymer backbone in the BNP. For this purpose, a calculated amount of $FeCl_3$ was then simply added to a methanolic suspension of BNP. The reaction scheme and the MOP formation are illustrated in Figure 1a. Upon addition of $FeCl_3$, the color of the solution immediately changed and the formation of nanoparticles with distinct contrast between the center and corona were evident from TEM (Figure 1b and 1c). This provided the first indication of the hollow nature of the resultant nanoparticles. The hollow morphology was further investigated using field emission scanning electron microscopy (SEM, Figure 1d). Broken nanoparticles indeed showed empty inner spaces (inset of Figure 1d), providing direct evidence for the formation of hollow nanoparticles.

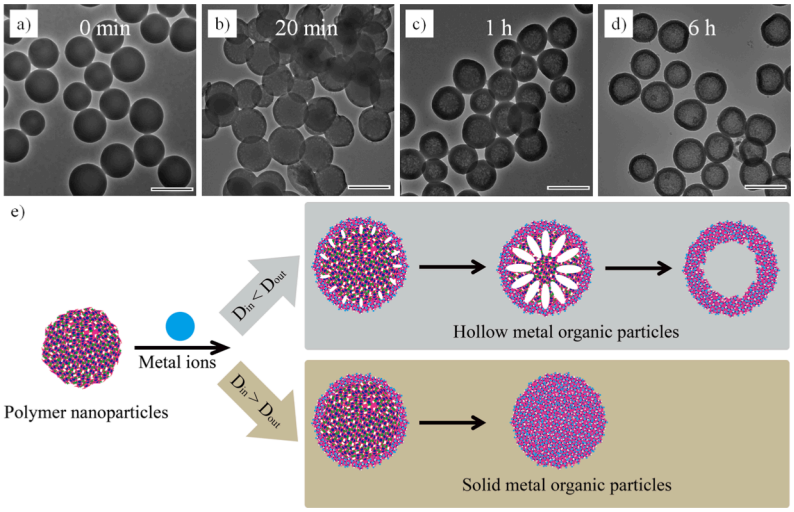

Figure 2. Morphology change during the hollow particle formation against time.. TEM images were taken at a) 0 min, b) 20 min, c) 1 h and d) 6 h after the addition of $FeCl_3$ into BNP; the scale bar is 500 nm. Conditions: 0.1 mL $FeCl_3$ methanol solution was added into 1 mL BNP methanol solution prepared using 3 mg/mL Im-BA and Im-Ca, the ratio of Fe^{3+} to Im-Ca was 1/2. The TEM samples were taken by drop-casting. e) Schematic illustration showing the transformation of solid polymer nanoparticles to hollow or solid metal organic particles, depending on the relative diffusivities.

To probe the mechanism of the hollow MOP formation, we monitored the temporal evolution of the conversion of the BNPs to hollow MOPs after addition of $FeCl_3$. A few small cavities in interior of the solid nanoparticles (Figure 2b) are clearly observed within 20 minutes. After 1 hour, the particle cores became patchy and the surface of the nanoparticles became

concurrently more prominent (Figure 2c). Fully hollow nanoparticles were formed after 6 hours (Figure 2d) and no further evolution of morphology was observed after 19 hours, suggesting that hollow nanoparticles were stably formed in solution. A reasonable hypothesis is that the formation of hollow MOPs is controlled by the relative diffusion of the reactive species on to the surface of the nanoparticle, which form the interface between the reacting species. Such a mechanistic possibility is reminiscent of the Kirkendall effect, albeit in a very different format, which has been utilized in metallurgy and hollow inorganic oxides and sulfides.

An important implication of understanding the operating mechanism is that it offers a pathway for additional control elements. The proposed mechanism for the formation of hollow MOPs would suggest that the diffusion of the boronate ester polymer to the surface of the nanoparticle, where the reaction between Fe^{3+} and the boronate ester takes place, is faster than the diffusion of Fe^{3+} from the solution to the interior of the particle (Figure 4e). If the opposite were true (diffusion of Fe^{3+} into the interior of the BNP is faster than boronate ester polymer out-diffusion), then the resultant product will be a solid nanoparticle. We hypothesized then that one can gain control over the thickness of the shell in the hollow MOPs by simply tuning the concentration of Fe^{3+} in solution, as these variations will generate an intermediate scenario between the solid and the hollow nanoparticles. Accordingly, the ratio of metal ions to the polymer repeat units was varied. Indeed, this variation was found to affect not only the thickness of the shells, but understandably also the rate of the formation of the hollow MOPs. For example, when the concentration of $FeCl_3$ is 1/8th of that of the Im-Ca repeat unit in the polymer, it took more than 12 hours to complete the formation of hollow MOP. However, this process was completed within 2 hours, when this ratio was changed to 1:2. As anticipated, the thickness of the shell was also observed to increase consistently with the increasing ratio of $FeCl_3$/Im-Ca, from about 15 nm to 90 nm when the ratio increased from 1/8 to 3/4. The formation of solid MOPs in the presence of an even higher concentration of Fe^{3+} ions (ratio of $FeCl_3$/Im-Ca is 1:1) further supports the proposed mechanism. EDS analysis of the samples showed a homogenous distribution of element Fe in the respective solid nanoparticles.

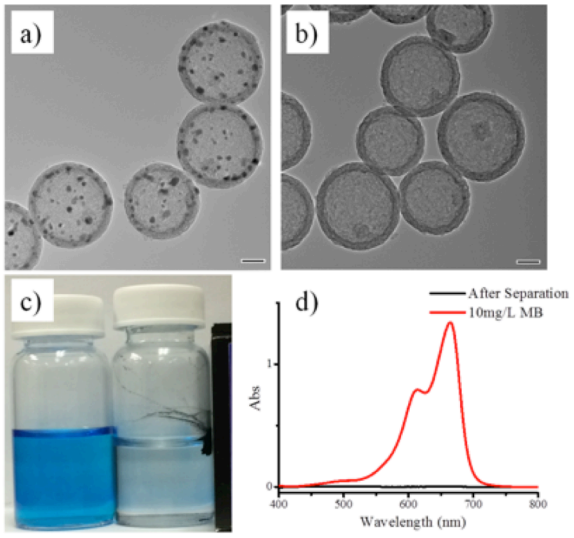

Figure 3. Preparation and application of hollow Fe@C particles. TEM measurement of a) hollow Fe@C particles after the temperature thermal treatment of MOPs, b) hollow carbon particles after the acid treatment of Fe@C; c) Optical photograph of the MB solution without (left) and with (right) the addition of Fe@C applying an external magnet; d) UV-vis absorption measurement before and after the magnetic separation.

To demonstrate a potential application of these hollow MOPs, hollow carbon particles loaded with metal nanoparticles (M@C) were prepared by direct pyrolysis. The advantage of such a system is that the hollow nature of the particles allows for molecular diffusion, while confiining the metal nanoparticles within them. To demonstrate such a possibility, the high temperature thermal treatment of hollow Fe^{3+}-MOPs at 800 ^{o}C under a N_2 atmosphere for 1 hour resulted in the formation of light color hollow carbon spheres loaded with small dark

nanoparticles as shown in TEM of Figure 3a. These carbon particles with encapsulated magnetic-Fe nanoparticles have been successfully used as a magnetically separable adsorbent for removing organic waste from aqueous solution using an organic dye (methylene blue, MB), as shown in Figure 3c and 3d.

In conclusion, a simple and versatile strategy for achieving hollow metal organic nanoparticles has been developed, where metal ions are simply added into solutions of boronate ester based solid organic nanoparticles. The size of the hollow MOPs is dictated by the size of the precursor BNP, which itself exhibits excellent tunability. The formation of these hollow MOPs seem to be independent of the valence and the geometry of the metal ion, which also allows for the incorporation of more than one type of metal ion into the MOPs. Interestingly, the underlying mechanism for the formation of these hollow MOPs seems to be controlled by the diffusion of the reactive species to the interface of the particle and the solution. This understanding further lends itself to control in the shell thickness of the MOPs. Overall, the method reported here for achieving hollow MOPs with a high degree of control has the versatility to impact applications such as catalysis, sensing, storage, and biomedicine, as this approach is extendable to other metal ions and potentially to other organic-inorganic molecular architectures.

Supramolecular dissociation strategy for sensing: Sensors for recognizing biological analytes are important due to the implications in proteomics, medical diagnostics, and pathogen detection. Approaches to developing new sensors can be broadly classified into two categories, both of which are inspired by nature: (*i*) array-based sensing, where several less-specific receptors are used to develop a response pattern for each analyte; and (*ii*) sensing based on 'lock-and-key' design, where specific receptors are needed to selectively bind the analytes of interest. The former method has the advantage of being simple as the receptor design is less intense and provides convenient opportunities to transduce the analyte recognition. In contrast, the latter approach has the promise of being specific to the target analyte even when the analyte mixture becomes complex. An approach that captures the simplicity of the former and the specificity of the latter would certainly be desirable for ultimately implementing these strategies in practical systems. Here, we demonstrate a simple supramolecular dissociation approach to protein sensing based on specific ligand-analyte interactions.

A sensor system requires two important elements, *viz.* specific recognition of the target analyte and generation of a signal that transduces the recognition event. Enabled by the efforts in drug discovery to impact pharma, specific ligands have been developed for many important proteins. However, methods that utilize these ligand discoveries to develop protein sensors are scarce, as these are hampered by strategies that transduce these binding events. Prior

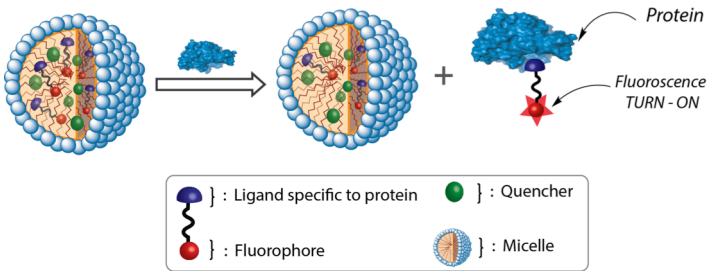

Figure 4. Schematic illustration of the supramolecular dissociation based protein sensor. The difference in the equilibrium concentrations (between the interior of the micelle and the bulk aqueous phase) of the pristine fluorescent probe and the probe-protein complex affords a simple, turn-on fluorescent sensor.

approaches that utilize these ligands require a supramolecular disassembly event to occur in response to a specific ligand-protein binding event. This strategy therefore requires a design strategy that requires the ligand-containing molecule to assemble in the absence of the protein, but disassemble in its presence. We envisaged a simple supramolecular dissociation strategy that obviates this rigorous design requirement (Figure 4). Briefly, in this approach, a probe is generated by simply tethering the protein-specific ligand moiety to a hydrophobic fluorophore, which is non-covalently incorporated into a micelle along with a corresponding hydrophobic fluorescence quencher. The micelle itself is chosen such that it is known to exhibit good guest exchange dynamics with the bulk solvent, *i.e.* the aqueous phase. Here, since the probe molecule is hydrophobic, its thermodynamic distribution coefficient will dictate that most of it is present inside the micelle, where the fluorescence is quenched due to its co-confinement with the quencher. We hypothesized that in the presence of the analyte protein, the binding event between the ligand moiety in the probe and the protein should cause the complex to decidedly favor the bulk solvent. This anticipation is because, in contrast to the probe by itself, the probe-protein complex should not have the hydrophobic driving force to re-bind to the interior of the micellar host. This specific protein-driven dissociation of the probe from the micelle also drastically decreases the proximity of the fluorophore and the quencher, which can be conveniently read as fluorescence increase, as schematically illustrated in Figure 4. The extent of this dissociation should also be dependent on the concentration of analyte protein.

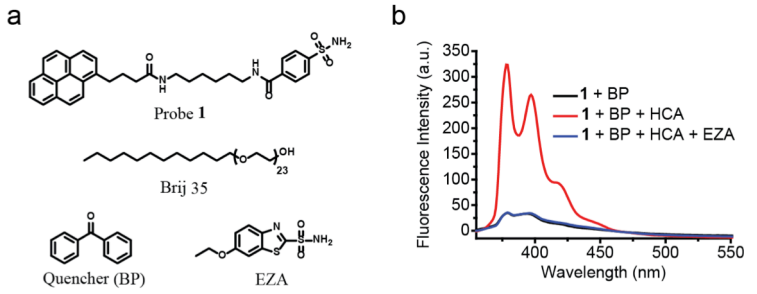

Figure 5. (a) Chemical structures of probe **1**, quencher and micelle. (b) Fluorescence spectra of probe **1** (1 μM) and benzophenone (5 mM) in Brij 35 (1 mM) Tris buffer solution (25 mM, pH 7.4) treated without or with HCA (5 μM) or with HCA (5 μM) and EZA (100 μM). All spectra were taken after 3-hour HCA incubation at room temperature.

To test our design hypothesis, we chose human carbonic anhydrase I (HCA) as the target analyte because of its disease relevance. Brij 35, a commercially available surfactant, is used as the micelle-forming macromolecule because its non-ionic head group, composed of polyethylene glycol unit, helps reduce nonspecific interactions. Benzenesulfonamide, which is used as a specific ligand to bind HCA, is tethered to pyrene as the fluorophore using a simple hydrophobic linker to obtain the fluorescent probe **1** (Figure 5a). Benzophenone was used as the quencher.

When HCA was added to the Brij 35 micellar assembly containing probe **1** and BP, the fluorescence of pyrene increased dramatically (Figure 5b). To check if this fluorescence enhancement is indeed due to the ligand-protein binding mechanism illustrated in Figure 4, we added a competitive ligand to HCA. The presence of the competitive ligand should displace the fluorescent probe from the protein. Since the probe is hydrophobic, it should be re-encapsulated into the micelle upon release from the protein to cause the fluorescence to be quenched again. As shown in Figure 5b, addition of 6-Ethoxy-2-benzothiazolesulfonamide (EZA), a strong competitive inhibitor of HCA, caused the fluorescence to go back to the original fluorescence level, *i.e.* significantly quenched. In addition to supporting the design hypothesis outlined in Figure 4, this observation also suggests that the micellar assembly itself is intact and that the BP

quencher stays encapsulated in this assembly to cause the re-encapsulated fluorophore to be quenched.

Through a series of control experiments, we have confirmed the mechanism of sensing in this approach. The versatility of this approach lies in its simplicity: (*i*) well-established and commercially available surfactants can be used; (*ii*) other than being hydrophobic, the fluorophore-ligand combination does not have to exhibit inherent self-assembly features and therefore does not require extensive molecular design; (*iii*) the strategy is conveniently extendable to any fluorophore-quencher combinations to modulate the colour of detection; and (*iv*) the approach is potentially extendable to most target protein analytes. Overall, we anticipate that the design principle has the potential to open up fundamentally new avenues in supramolecular chemistry for generation of fluorescent signal or even other spectroscopic signals in response to specific protein-ligand recognition events.